Soft-Lithographed Up-Converted Distributed Feedback Visible Lasers Based on CdSe–CdZnS–ZnS Quantum Dots

*Francesco Todescato, Ilaria Fortunati, Samuele Gardin, Eleonora Garbin, Elisabetta Collini, Renato Bozio, Jacek J. Jasieniak, Gioia Della Giustina, Giovanna Brusatin, Stefano Toffanin, and Raffaella Signorini**

The development of a solution-deposited up-converted distributed feedback laser prototype is presented. It employs a sol–gel silica/germania soft-lithographed microcavity and CdSe–CdZnS–ZnS quantum dot/sol–gel zirconia composites as optical gain material. Characterization of the linear and nonlinear optical properties of quantum dots establishes their high absorption cross-sections in the one- and two- photon absorption regimes to be 1×10^{-14} cm^2 and 5×10^4 GM, respectively. In addition, ultrafast transient absorption dynamics measurements of the graded seal quantum dots reveal that the Auger recombination lifetime is 220 ps, a value two times higher than that of the corresponding CdSe core. These factors enable the use of such quantum dots as optically pumped gain media, operating in the one- and two-photon absorption regime. The incorporation of CdSe–CdZnS–ZnS quantum dots within a zirconia host matrix affords a quantum-dot ink that can be directly deposited on our soft-lithographed distributed feedback grating to form an all-solution-processed microcavity laser.

1. Introduction

The rapid advancement in the miniaturization of laser technologies is permitting the development of novel and improved devices in areas such as telecommunications, computing, and sensing.[1–4] Conventional laser technologies rely mainly on solid-state active materials operating in the infrared (IR) region of the spectrum. In addition to their widespread use in telecommunication, IR lasers are broadly used in optical recording and image processing. For many applications, however, ultraviolet (UV) or visible laser radiation is required. To accomplish this, the IR source is conventionally converted to higher energies by way of second-harmonic generation, or frequency doubling, within bulk crystals of, for example, β-barium borate (BBO)[5] or potassium dihydrogen phosphate (KDP).[6]

An alternative method is to utilize up-conversion emission following a multi-photon absorption mechanism. In this process, virtual absorption states are populated before being re-excited by additional photons. This allows for optical absorption to occur in a spectral range where the one-photon absorption coefficient is negligible. In this manner, IR radiation can be absorbed by a material that emits at higher energy. The key criteria to develop efficient up-converting materials are: i) high two-photon absorption (TPA) efficiencies; ii) high fluorescence quantum yields (FQY); iii) high gain coefficients; and, iv) high chemical and photo-stabilities under laser irradiation.[7] While the multi-photon absorption properties of many organic and inorganic materials have been widely studied, few have satisfied these requirements as well as multi-shell inorganic semiconductor quantum dots (QDs).[8–10]

One of the most lucrative properties of QDs is their size-tunable photoluminescence (PL) wavelength. This is particularly beneficial for developing up-converted lasers from a single material.[11,12] When QDs are pumped into high-energy excited states, population inversion and build-up of optical gain take place. This allows for spontaneous emission to be amplified through a process called amplified spontaneous emission (ASE). High ASE yields can be reached when nonradiative processes, such as surface trapping and Auger recombination, are reduced and the optical gain is maximized.[13,14] This can be achieved by using graded shell quantum dot architectures.[15–17] When coupled with suitable microcavities, such as microring, spherical resonators,[18–20] distributed Bragg reflectors,[21] and distributed feedback (DFB),[22–24] the optical gain which stems from QDs can be exploited to develop prototype QD based microlasers.

In this study, we employ a second-order DFB structure, fabricated through soft-lithography, to develop a QD laser prototype that operates in the visible region of the electromagnetic spectrum. By harnessing both the linear and nonlinear optical

Dr. F. Todescato, Dr. I. Fortunati, Dr. S. Gardin, Dr. E. Garbin, Dr. E. Collini, Prof. R. Bozio, Dr. R. Signorini
Department of Chemical Science and U.R. INSTM
University of Padova
Via Marzolo 1, I-35131, Padova, Italy
E-mail: raffaella.signorini@unipd.it
Dr. J. J. Jasieniak
CSIRO Division of Materials Science and Engineering Ian Wark Laboratory
Bayview Avenue, Clayton 3168, Australia
Dr. G. Della Giustina, Dr. G. Brusatin
Department of Mechanical Engineering
Materials Section and U.R. INSTM
University of Padova
Via Marzolo 9, I-35131 Padova, Italy
Dr. S. Toffanin
CNR, ISMN
Via Gobetti 101, I-40129 Bologna, Italy

DOI: 10.1002/adfm.201101684

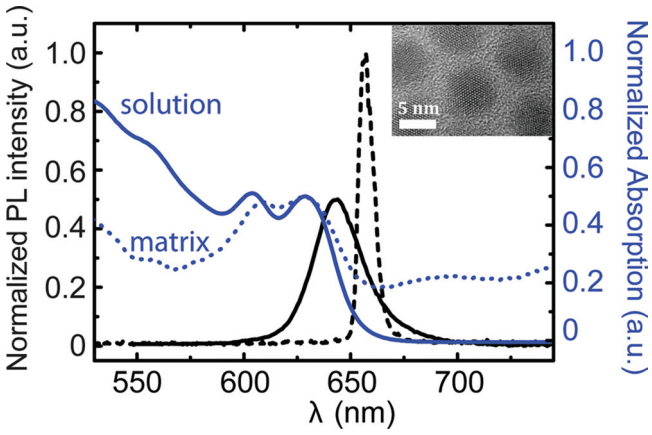

Figure 1. Linear optical properties of QDs: normalized absorption in EtOH solution (blue line) and in zirconia matrix (blue dashed line), normalized emission (black line), and ASE (black dashed line) in matrix. HRTEM of CdSe–CdZnS–ZnS multishell QDs (inset).

properties of QDs, we show that this laser can be effectively operated through optically pumping either by UV–Visible (through one-photon absorption) or near-IR (up-converted two-photon absorption) radiation.

2. Results and Discussion

2.1. Linear and Nonlinear Absorption Characteristics

In this work we utilized CdSe–CdZnS–ZnS QDs as optical gain active material for lasing. QDs were composed of 5.3 nm CdSe cores which were overcoated by a 1.2 nm thick CdZnS–ZnS graded shell.[25] Linear and nonlinear optical characterizations of QDs were performed in ethanol (EtOH) solution and in solid films. As shown in **Figure 1**, the band-edge exciton absorption peak of the QDs in solution occurs at 629 nm. Through quantitative renormalization of published extinction coefficient data during the shell deposition, we determine the band-edge extinction coefficient at this wavelength to be 4.5×10^5 M^{-1} cm^{-1} corresponding to a one-photon absorption cross-section (σ_0), at 400 nm, of 1.1×10^{-14} cm^2.[26] The spontaneous fluorescence emission is red-shifted to 638 nm, with a FWHM of about 30 nm. An FQY of (35 ± 1)% is measured, following the procedure described by Demas and Crosby,[27] using Cresyl Violet in methanol (FQY = 0.66) as a standard.[27] To utilize such QDs as the active component of an optical gain layer, it is necessary for them to be dispersed at mM concentrations within the layer. We have previously shown that a zirconia based sol–gel matrix is a suitable host for our graded NCs because it forms a type-I electronic configuration.[28] This hybrid system possesses a high refractive index and retains high photostability under one- and two-photon pumping, important peculiarities for developing QD-based DFB lasers.[29]

Thin films of densely packed CdSe–CdZnS–ZnS QDs in a zirconia host were deposited, by spin-coating, onto quartz substrates. A comparison of the absorption and emission properties of the QDs dispersed in EtOH and QD/ZrO_2 thin films is shown in Figure 1 (blue line and blue dashed line, respectively). The first absorption peak of QDs in the thin film and in solution is centered at the same wavelength. However, this observation is by coincidence only, as interference effects have not been considered here. The presence of interference can be clearly seen from the markedly different absorption of the film profile at longer wavelengths. In densified QD films, where the local refractive index and the extent of electronic coupling have increased, a bathochromic shift of the absorption and photoluminescence peaks are expected. Indeed, a red-shift of the fluorescence from 638 to 644 nm is observed, with FWHM (full width at half maximum) of approximately 26 nm. The fluorescence quantum yield of a 245 nm thick sample, measured with an integrating sphere,[30] exhibits an efficiency of (7.3 ± 0.2)%. The reduced FQY efficiency of the QDs in zirconia is likely due to low-energy lying nonemissive surface trap states, created by the annealing process.[28,31]

Nonlinear optical characterization of QDs was performed using the two-photon induced fluorescence (TPIF) and open-aperture *z*-scan techniques. The TPA cross section (σ_{TPA}) of QD solution, measured by TPIF, exhibits remarkably high values, ranging between 33 000 and 53 000 GM, where 1 GM = 10^{-50} cm^4 s $photon^{-1}$; at 800 nm its value is 44 900 GM (the TPA spectrum is reported in the Supporting Information). Since TPIF cannot be performed on solid state samples,[32] the *z*-scan technique was used, according to the method proposed by Sheik-Bahae et al.[33]

With *z*-scan measurements the two photon absorption coefficients of QDs in thin film and solution are determined at 800 nm, giving 1.98 cm GW^{-1} and 1.54×10^{-2} cm GW^{-1}, respectively. The magnitude of these TPA coefficients is comparable to literature data on solution and close-packed QD samples.[34,35] The corresponding σ_{TPA} is 21 000 ± 4 700 GM in the thin-film, a value similar to that obtained in solution (16 000 ± 1400 GM). Consistent with previous reports, the TPA cross-sections measured with *z*- scan are smaller than the ones measured by TPIF[36].

2.2. Ultrafast e–h Dynamics of CdSe-CdZnS-ZnS QDs

To employ QD based thin-films in laser devices, it is important to understand the dynamics of the electronic states involved in the optical amplification process. Femtosecond transient absorption (TA) is a well-suited technique to investigate the build-up and the decay kinetics of such states.[37,38] Optical gain can be observed in TA spectra as a negative variation of induced absorption (absorption bleach, $\Delta\alpha < 0$) with a magnitude greater than the linear absorption (α_0), so that $-\Delta\alpha/\alpha_0 > 1$. Thin-films of QDs in a zirconia host with different thicknesses were studied using a 150 fs pump beam at 400 nm and a variably delayed fs white light continuum probe. **Figure 2** shows the nonlinear absorption spectra ($\alpha = \alpha_0 + \Delta\alpha$) of a 245 nm thin-film recorded at 1.5 ps delay time with different excitation fluences. The carrier density $N_{e\text{-}h}$ corresponds to the average number of e–h pairs per dot; it is directly proportional to the exciting pump beam fluence through the relation $N_{e\text{-}h} = j_p \cdot \sigma_0$, where j_p is the pump fluence and σ_0 is the QD absorption cross-section.[39] The data show that in the investigated spectral

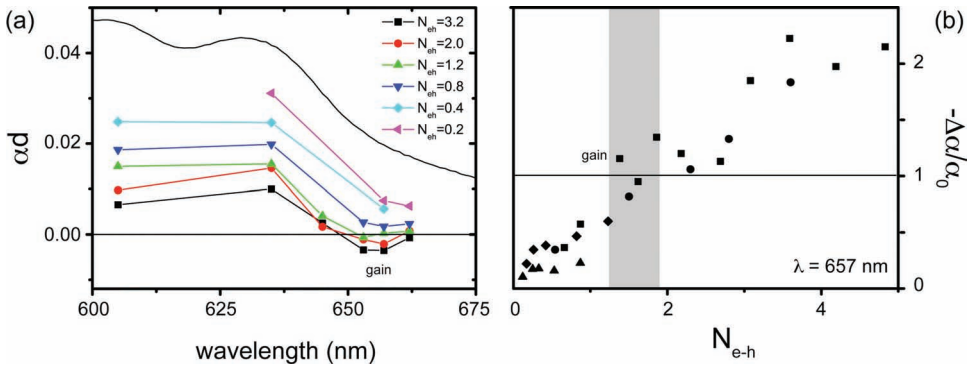

Figure 2. a) Nonlinear absorption spectra recorded at 1.5 ps delay time for a 245 nm QD/ZrO_2 film as a function of carrier density. Optical gain is observed around 657 nm where $\alpha = \alpha_0 + \Delta\alpha < 0$. b) Pump dependence of normalized absorption changes ($-\Delta\alpha/\alpha_0$) measured at 657 nm. Different symbols correspond to measurements on different films. The threshold of optical gain process is estimated around $N_{e\text{-}h} \approx 1.5$ (shadowed area).

range the transient signal of the first absorption band is dominated by bleaching. This observation has been correlated to the state-filling of the 1S(e) electronic level of the CdSe core.[40] On the red side of this bleached absorption band however, which corresponds spectrally to the position of the emission band, a crossover from absorption to optical gain is observed at higher pump fluences.

In Figure 2b the normalized absorption changes $-\Delta\alpha/\alpha_0$ of this optical gain band are probed as function of carrier density. The threshold for the optical gain ($-\Delta\alpha/\alpha_0 > 1$) is estimated to be around $N_{e\text{-}h} \approx 1.5$ on average, in good agreement with previous measurements on CdSe QDs.[29,37] This value is consistent with the population-inversion mechanism in a simple model system proposed by Klimov.[38] In such a system, where more than one electron–hole pair is created on average, the optical gain and consequently the amplified spontaneous emission originate from the relaxation between the biexcitonic and the single exciton states. The single exciton decays naturally through spontaneous or nonradiative emission.[29]

In order to understand the ultrafast dynamics of the optical state, **Figure 3**a shows traces of the carrier-induced absorption changes ($-\Delta\alpha$) vs. delay time for increasing values of carrier density. In the regime of multiple e–h pair excitation, the radiative decay of excited states is limited by the Auger recombination process.[37] These Auger rates have been found to drastically increase with an increasing e–h pair population and decrease in quantum dot size. The determination of the Auger rate constants is fundamental in order to evaluate the efficiency of specific nanocrystals for application in lasing technologies. It is well known that competition between radiative and nonradiative (Auger) processes critically affects optical gain. Novel nanocrystal hetero-structures, which possess rapid radiative rates but have suppressed Auger recombination rates, are in great demand for the practical application of quantum dots in future lasing devices.[41] The analysis of Auger recombination rates was done following the procedure and the notation introduced by Klimov et al.[38] The QD-based thin films show an exceptionally long lifetime of the bi-excitonic state, $\tau_2 \approx 220$ ps. This time constant is more than two times that previously measured for 5.3 nm sized CdSe cores with and without a ZnS shell.[39,40] Consistent with the multiexcitonic origin of optical amplification in QDs, temporal analysis of the optical gain state for these samples shows that it is sustained for more than 100 ps (Figure 3b). The magnitude of this optical gain lifetime is comparable with values determined for core–shell quantum rods which have been specifically designed to suppress the rate of Auger recombination.[42] Further investigations are underway to understand the role of the host matrix and the nature of the QD heterostructure in this enhanced Auger lifetime.

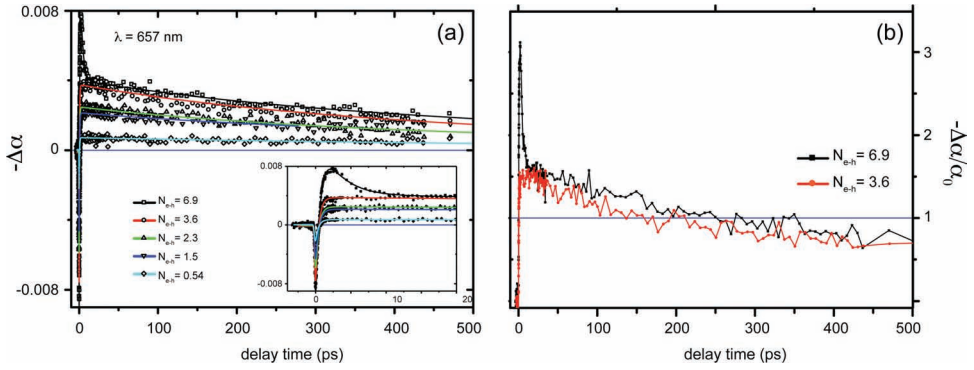

Figure 3. a) Decay traces at 657 nm for a 326 nm QD/ZrO_2 film as a function of pump fluence. b) Time evolution of the normalized transient absorption ($-\Delta\alpha/\alpha_0$) measured at the peak of the gain for a 326 nm QD/ZrO_2 film at two different values of carrier density: the gain ($-\Delta\alpha/\alpha_0 > 1$) is sustained for more than 100 ps.

Table 1. Amplified spontaneous emission characteristics of QD/ZrO_2 samples with different thicknesses under one-photon and two-photon optical excitation.

	One-Photon Optical Excitation				Two-Photon Optical Excitation			
QD/ZrO_2 Thickness [nm]	Peak [nm]	FWHM [nm]	Threshold [mJ cm^{-2}]	Gain [cm^{-1}]	Peak [nm]	FWHM [nm]	Threshold [mJ cm^{-2}]	Gain [cm^{-1}]
150	657	9	0.229 ± 0.042	150	654	8	14.19 ± 0.73	184
245	657	9	0.185 ± 0.016	179	658	8	12.31 ± 0.85	178
326	659	8	0.173 ± 0.011	160	659	8	12.79 ± 0.85	161

2.3. Amplified Spontaneous Emission Properties

To exploit the improved optical gain behavior in our QD thin films, the ASE process is studied as function of the active layer thickness, under one- (at 400 nm) and two-photon (at 800 nm) excitation (**Table 1**). At low excitation fluences only spontaneous emission was detected, above the optical gain threshold a narrower (FWHM ≈ 8–9 nm) ASE contribution was observed (**Figure 4**a and c). The ASE of the QD/ZrO_2 peaked at about 657 nm, with a typical FWHM of about 9 nm and red-shifted with respect to the maximum of the emission band by about 40 meV. This is indicative of a biexciton state, where a negative interaction energy causes a red-shift of the biexciton resonance to a lower-energy with respect to that of single e–h pair emission.[43] For both one- and two-photon pumped cases, it can be noticed that a lowering of the threshold values occurs with increasing film thickness. For developing a laser however, it is vital that a balance between high optical gain efficiency and a low ASE threshold is reached. The determination of the effective gain coefficient, through the variable stripe (VSL) technique,[29] indicates a maximum of approximately 179 cm^{-1} for the 245 nm thick sample (Figure 4b and d). Based on this factor, and together with further theoretical insight reported below, we selected the 245 nm thick QD/ZrO_2 film as the best optical gain candidate for developing a 1-D DFB laser device.

2.4. Distributed Feedback Laser Properties

In order to transform the aforementioned cavity-less laser to a true laser, the optical gain medium must be incorporated into an appropriate cavity. In this work a DFB configuration has been employed as laser microcavity.[44,45] This type of structure is particularly interesting for the miniaturization of future laser technologies because of its simplicity and versatility in terms of different gain materials. The optical feedback is provided via Bragg scattering from a periodic perturbation of the refractive index (n) and/or of the gain coefficient (g). Particularly relevant

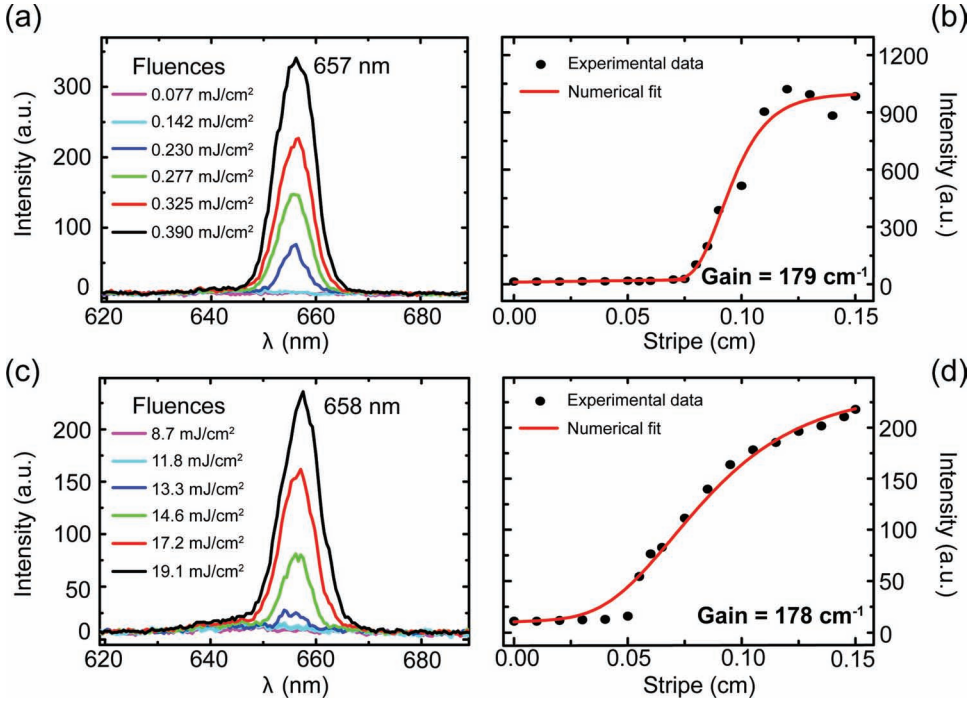

Figure 4. a) ASE emission signals for CdSe–CdZnS–ZnS/ZrO_2 waveguides under one-photon excitation at 400 nm, recorded at different input fluences. b) VSL measurements performed under 400 nm optical pumping, at 0.278 mJ cm^{-2}. c) ASE emission signals for CdSe–CdZnS–ZnS/ZrO_2 waveguides under two-photon excitation at 800 nm, recorded at different input fluences. d) VSL measurements performed under 800 nm optical pumping, at 17.2 mJ cm^{-2}. For both VSL measurement experimental data are fitted to an Auger limited 1-D amplifier model (red lines).

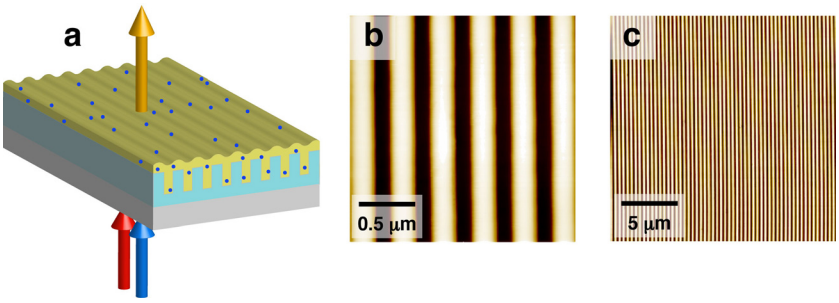

Figure 5. a) Pumping geometry for lasing characterizations. b) AFM measurement of 20 × 20 μm² of DFB grating, showing the large area uniformity of the structure. c) AFM measurement of 2 μm × 2 μm to check the quality of DFB grating.

to DFB lasers is the strong selectivity of the output cavity mode on the period of the modulation in the grating and on the thickness of the optical gain material.[45]

The emission wavelength in vacuum ($\lambda_{0,Br}$) of a DFB grating is given by the Bragg relation $\lambda_{0,Br} = \frac{2N\Lambda}{p}$, where N is the effective refractive index of the waveguide, Λ is the period of the grating and p is the grating order. For a second-order grating this equation becomes $\lambda_{0,Br} = N\Lambda$. We focused on a laser output coming from a second-order diffraction. Advantageously, in this case the laser emission direction is perpendicular to the surface of the DFB. This factor minimizes any adverse edge effects from experimental measurements.

The 1D Bragg grating prototype was prepared by imprinting of a suitable germania based sol–gel matrix (named G8Ge2).[46] This matrix has a refractive index of $n = 1.48$ and can be patterned with a commercial silicon master. The obtained samples show a uniform pattern over a large area of about 2 cm × 2 cm, with a 400 nm period and features depth of 200 nm. Atomic force microscopy (AFM) measurements ensure the high quality and uniformity of the grating over such a long range (**Figure 5**).

To transform the Bragg grating to a prototype laser, a QD-doped zirconia matrix was simply deposited on top of the corrugated surface. Lasing characteristics of the device were investigated following optical pumping by one- and two-photon excitation (Figure 5a). Initial investigations of a 158 nm thick QD/ZrO_2 film on our DFB presented lasing peaks at 627 and 635 nm for one- and two-photon pumping, respectively (**Figure 6**a and c). At low fluences only the spontaneous emission was detectable, however by increasing the input energy above the lasing thresholds (reported in **Table 2**, and Figure 6b and d), true laser emission was observed. The laser lines exhibited a FWHM below the resolution limit of 1 nm of the detection system used. The increase of the QD/ZrO_2 film thickness to 245 nm, resulted in two different lasing peaks, both for one- and two-photon excitation (**Figure 7**a and c). Polarization experiments have shown that these peaks correspond to different polarization modes: the laser line at 652 nm is a TM mode (with electric field polarized perpendicular to the grating grooves) and the laser line at 662 nm is a TE mode (with polarization in the plane of incidence parallel to the grating grooves).[47] The threshold fluences are 0.077 ± 0.023 (Figure 7b) and 0.108 ± 0.056 mJ cm^{-2} for the one-photon pumped TM and TE modes respectively, and 8.3 ± 2.5 (Figure 7d) and 11.4 ± 3.2 mJ cm^{-2} for the up-converted lasing.

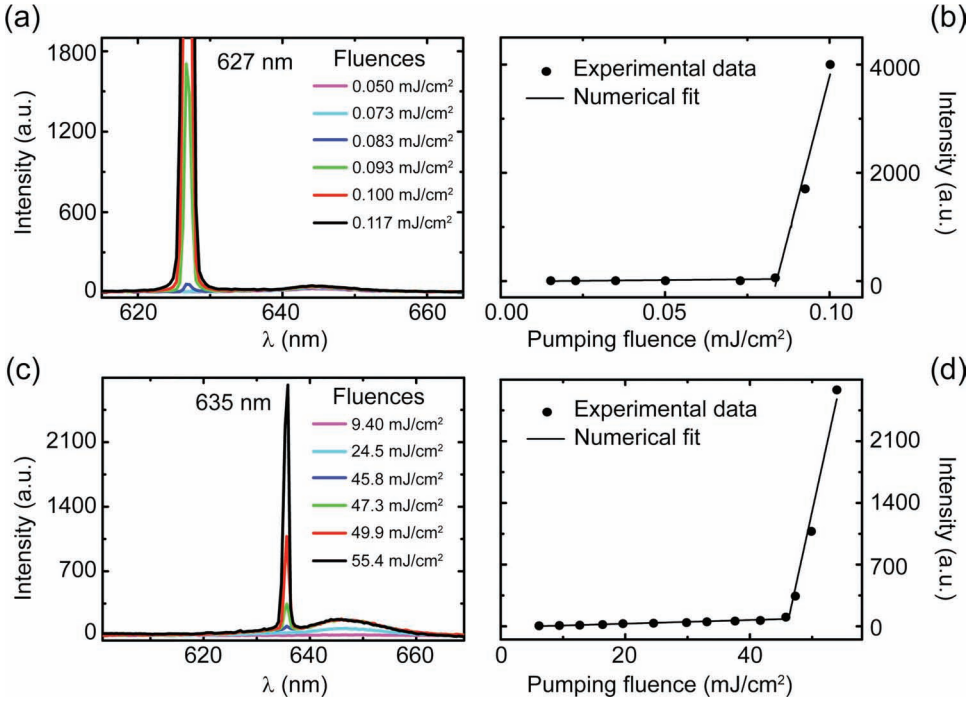

Figure 6. Emission of the 150 nm thick prototype at increasing fluences pumped at 400 (a) and 800 nm (c) with relative peak intensity (b,d). The lasing peak appears above thresholds of 0.083 mJ cm^{-2} (b) and 47.8 mJ cm^{-2} (d) for one- and two-photon pumping, respectively.

Table 2. Lasing peaks position and threshold for one- and two-photon pumped prototype with different active material thickness.

Pumping beam [nm]	Mode	Thickness [nm]	Peak [nm]	FWHM [nm]	Threshold [mJ cm^{-2}]
400	–	150	627	<1	0.083 ± 0.01
800	–	150	635	<1	47.8 ± 4.1
400	TM	245	652	<1	0.077 ± 0.023
400	TE	245	662	<1	0.108 ± 0.056
800	TM	245	652	<1	8.3 ± 2.5
800	TE	245	662	<1	11.4 ± 3.2

The lasing peak shift, with increasing film thickness, is due to different optical modes sustained within the optical gain material: thinner waveguides allow more energetic modes.[45] The lasing peak observed in the 150 nm film is strongly blue-shifted, as compared to the ASE maximum. The presence of laser emission, despite the mismatch of the resonant wavelength in the cavity with respect to the ASE peak, suggests that the optical gain is spectrally broad enough to exhibit lasing in this region. The exact position of the cavity modes depends strongly on the periodicity of the grating,[45] and in our case is designed to center the laser emission at 650 nm when 250 nm thick active material is used. In this case, the laser emission is resonant with the optical gain maximum of QDs. As a result, the enhanced feedback efficiency for the 245 nm thick QD/ZrO_2 film involved a significant reduction in the lasing threshold compared to the 150 nm sample.

The experimental lasing peak wavelengths are compared with the calculated ones obtained for a 1-D DFB structure, in which the second-order Bragg equation was solved considering film thicknesses of 150, 245, and 326 nm and a 400 nm grating period (see the Supporting Information for details). The calculated DFB wavelengths were 639, 659, and 670 nm for the three different optical gain layer thicknesses, respectively, in good agreement with the experimental results.

To further assess the viability of our prototype lasers, we studied their bleaching dynamics under a continuous irradiation time at 1 kHz repetition rate in air. One-photon optical pumping resulted in an excellent stability over 1 h of continuous irradiation. Under two-photon pumping the stability behavior is slightly different. The lasing peak intensity was stable for the initial 20 min and underwent a subsequent reduction, reaching 50% of the original value after 50 min of irradiation (see the Supporting Information). All these measurements were conducted in air, thus it is anticipated that the stability of these devices under both one- and two-photon pumping should be remarkably enhanced through simple encapsulation methods.

3. Conclusions

We have explored the fabrication of a solution-processable distributed feedback laser. By combining the simplicity of sol–gel chemistry with the favourable luminescence and optical gain properties of CdSe–CdZnS–ZnS QDs, a DFB laser prototype was demonstrated. It emits in the visible range operating through a conventional one-photon excitation and the up-conversion of IR radiation. The analysis of the linear and non-linear absorption characteristics, as well as the Auger rates and the QD optical gain state dynamics, showed that all the requirements for the realization of a performing DFB laser were well

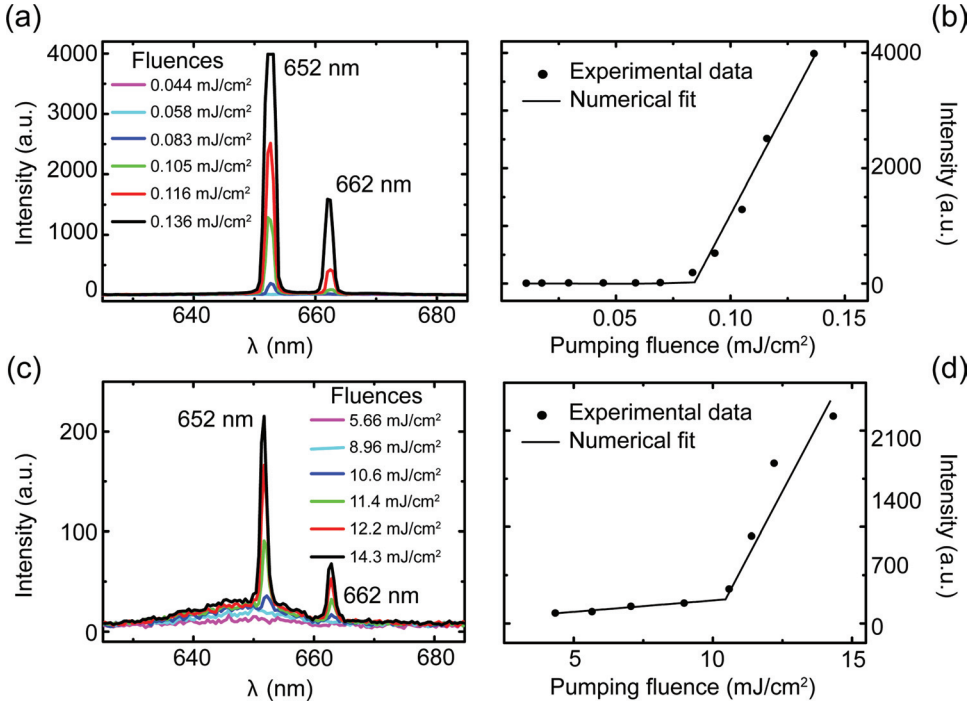

Figure 7. TM and TE emission of the 245 nm thick prototype at increasing fluences pumped at 400 (a) and 800 nm (c). The TM lasing peaks appear above thresholds of 0.077 ± 0.023 mJ cm^{-2} (b) and 8.3 ± 2.5 mJ cm^{-2} (d) for one- and two-photon pumping, respectively.

satisfied. Overall, the versatility of the laser configuration here demonstrated, opens the way to produce emission tunable compact lasers that can be easily integrated in today and tomorrow optical devices and sensing applications.

4. Experimental Section

Materials: The CdSe cores are prepared by the method reported by van Embden et al.[25] Core–shell nanocrystals are made following the recently developed SILAR method.[48–50] The final core–shell structure of the sample studied here, with the corresponding number of monolayers (ML), is: CdSe–CdS(1 ML)–$Cd_{0.5}Zn_{0.5}S$(1 ML)–ZnS(1 ML) (herein called CdSe–CdZnS–ZnS).

Post-synthesis, the nanocrystals are solubilized in ethanol through a 5-aminopentanol and tris-hydroxyphosphine surface exchange ready for incorporation into a sol–gel matrix.[29]

For the preparation of the ZrO_2-based sol–gel host, Zr-isopropoxide is used as the matrix precursor. It is mixed with acetylacetone in a molar ratio 1:1, used as chelating agent, and isopropanol as solvent. The solution is magnetically stirred for 1 h and then passed through a 0.2 μm PTFE filter before mixing with the appropriate amount of the QD solution. The QDs are dispersed in ethanol at a concentration of approximately 80 μM. For the doped solution, 100 μL of sol–gel solution is mixed with 200 μL of the QD solution. This sol is then spin-coated onto quartz glasses or patterned substrates at 3500 rpm for 20 s in Ar atmosphere to prevent degradation. Films are treated at 100 °C for 2 min and at 250 °C for a further 5 min. The final films for ASE and lasing measurements are prepared by depositing 2, 3, or 4 individual layers, as described above.

The G8Ge2 solution was prepared under acidic conditions, using 3-glycidoxypropyltrimethoxysilane (GPTMS) and germanium tetraethoxide (TEOG) as precursors, with relative molar ratio GPTMS/TEOG = 8:2 (as described in reference[46,51]) in an acidic environment. Films were spin coated on quartz substrates (n = 1.45) to obtain films with thickness of approximately 2 μm for imprinting.

The 1D pattern was realized by imprinting with a commercial silicon master possessing a period of 406 nm and features depth of 200 nm. The pattern replication was performed with the application of a pressure of 3 kN and treating the sample at 120 °C during the imprinting procedure.

Optical Experiments: The UV–visible absorption spectra are recorded using a Cary 5 spectrometer (Varian) in the range 350–800 nm. The fluorescence spectra are measured with a FluoroMax P (Jobin-Yvon) fluorimeter in the 550–750 nm range.

Solid-state quantum yield measurements were carry out inside a 6" Sphere Optics integrating sphere exciting the samples with the 375 nm emission of an Oxxius laser diode and collecting the signals with a calibrated optical multichannel analyzer (PMA-11, Hamamatsu).

Ellipsometric measurements are performed using a VASE32 J. A. Wollam Co. instrument at different incident angles (65°, 70°, and 75°). Wavelength steps of 5 nm are used to sweep the 300–1300 nm range.

Nonlinear experiments are performed using two different fs lasers. For TPIF experiments a tunable Ti:Sapphire laser system delivering 150 fs pulses at 76 MHz repetition rate is used.

The TPIF excitation spectra are recorded from 740 to 930 nm, with 10 nm steps. The laser beam was focused on the sample cell (a 10 mm quartz cell), via a 40 cm focal length lens. Fluorescence spectra excited by one- and two-photon excitation are in the same spectral region, confirming that the emitting states are the same for both processes. Therefore we assume the same FQY for both one- or two-photon excitation. TPA cross sections were evaluated following the procedure described in the literature[52] using an approximately 10^{-5} M solution of fluorescein in water at pH > 10 (0.1 M NaOH) as a reference standard. The concentrations used for the solutions are in the range 2×10^{-6} to 2×10^{-5} M.

Pump&Probe, *z*-scan, ASE and lasing emission are performed with an amplified Ti:Sapphire laser system. It delivers 150 fs pulses, with a maximum of 0.7 mJ per pulse energy, at approximately 800 nm and a repetition rate that is variable between 1 kHz and 10 Hz. With a BBO doubling crystal, a 400 nm wavelength beam is obtained. The intensity of the input beam is continuously varied with a half-wave plate in series with a polarizer, and a set of neutral density filters. The spatial profile of the input beam was measured using a CCD camera (Pulnix TM-7CN), placed on the beam focus, and the pulse energies are sampled with a pyroelectric detector (Molectron J3-05).

Z-scan experiments are performed at 800 nm, using a repetition rate of 200 Hz and a 100 mm focal length lens. The QDs solution used in the measurement has a concentration of about 4×10^{-5} M in a cell with 0.1 mm optical path. The thickness of the film was 590 nm.

In the Pump&Probe experiment, the samples are pumped at 3.1 eV (400 nm) by the frequency-doubled output of the amplified Ti:sapphire laser. The pump-induced absorption changes are probed at selected significant wavelengths over the range 600–700 nm with a femtosecond white-light continuum (WLC) generated in a sapphire window. In order to obtain chirp-free, high-sensitivity detection of TA signals, a single-wavelength phase-sensitive detection scheme is implemented: after the sample, the probe beam is focused into an optical fiber coupled with a monochromator and the signal at the selected wavelength is then detected by a Si photodiode and averaged by a digital Lock-In amplifier (Stanford Research SR830). All the experiments are carried out with a cross-polarized Pump&Probe configuration in order to eliminate any contribution from "coherent artefacts" at early times. More details about the Pump&Probe setup and data collection can be found in reference[53].

For ASE measurements the input beam is focused with a 200 mm focal length cylindrical lens onto the slide samples. The sample's edge emitted beam is detected in a lateral configuration by an optical fiber connected to a microspectrometer (Ocean Optics HR2000).

For lasing measurements the input beam is focused with a 100 mm spherical focal lens onto the slide samples. The sample is back illuminated and the emitted signal is recorded with a 0° geometry, using the optical fiber connected to microspectrometer, a cut off filter is used to remove the residual pumping laser beam. The device emission was detected in a plane parallel to the grating grooves containing the exciting beam (Figure 5a).

Supporting Information

Supporting Information is available from the Wiley Online Library or from the author.

Acknowledgements

Acknowledgments are due to PRAT_2010 project prot. CPDA104332/10 of University of Padova. J.J.J. acknowledges the Australian Research Council for support through the APD grant DP110105341. The authors are grateful also to Prof. C. Ferrante for stimulating discussions.

Received: July 21, 2011
Revised: September 29, 2011
Published online: November 17, 2011

[1] R. Dorn, D. Baums, P. Kersten, R. Regener, *Adv. Mater.* **1992**, *4*, 464.
[2] K. Itoh, W. Watanabe, Y. Ozeki, *Proc. IEEE* **2009**, *97*, 1011.
[3] G. Giuliani, M. Norgia, S. Donati, T. Bosch, *J. Opt. A: Pure Appl. Opt.* **2002**, *4*, S283.

[4] R. L. Bayer, *IEEE J. Sel. Top. Quantum Electron.* **2000**, *6*, 911.
[5] D. N. Nikogosyan, *Appl. Phys. A* **1991**, *52*, 359.
[6] M. Aoyama, T. Harimoto, J. Ma, Y. Akahane, K. Yamakawa, *Opt. Express* **2001**, *9*, 579.
[7] T. C. Lin, S. J. Chung, K. S. Kim, X. P. Wang, G. S. He, J. Swiatkiewicz, H. E. Pudavar, P. N. Prasad, in *Polymers for Photonics Applications II*, Advances in Polymer Science, Vol. 161, Springer-Verlag, Berlin **2003**, p. 157.
[8] A. Piryatinski, S. A. Ivanov, S. Tretiak, V. I. Klimov, *Nano Lett.* **2007**, *7*, 108.
[9] M. Achermann, M. A. Petruska, D. D. Koleske, M. H. Crawford, V. I. Klimov, *Nano Lett.* **2006**, *6*, 1396.
[10] R. D. Schaller, V. M. Agranovich, V. I. Klimov, *Nat. Phys.* **2005**, *1*, 189.
[11] F. Todescato, I. Fortunati, S. Gardin, R. Signorini, R. Bozio, J. J. Jasieniak, A. Martucci, G. Della Giustina, G. Brusatin, M. Guglielmi, *Proc. SPIE* **2010**, *7582*, 75821C.
[12] I. Fortunati, R. Signorini, R. Bozio, J. J. Jasieniak, A. Antonello, A. Martucci, G. Della Giustina, G. Brusatin, M. Guglielmi, *J. Phys. Chem. C* **2011**, *115*, 3840.
[13] V. I. Klimov, *Annu. Rev. Phys. Chem.* **2007**, *58*, 635.
[14] G. A. Turnbull, P. Andrew, M. J. Jory, W. L. Barnes, I. D. W. Samuel, *Phys. Rev. B* **2001**, *64*, 125122.
[15] J. McBride, J. Treadway, L. C. Feldman, S. J. Pennycook, S. J. Rosenthal, *Nano Lett.* **2006**, *6*, 1496.
[16] A. D. Lad, P. P. Kiran, G. R. Kumar, S. Mahamuni, *Appl. Phys. Lett.* **2007**, *90*, 133113.
[17] X. H. Wang, Y. M. Du, S. Ding, Q. Q. Wang, G. G. Xiong, M. Xie, X. C. Shen, D. W. Pang, *J. Phys. Chem. B* **2006**, *110*, 1566.
[18] A. V. Malko, A. A. Mikhailovsky, M. A. Petruska, J. A. Hollingsworth, H. Htoon, M. G. Bawendi, V. I. Klimov, *Appl. Phys. Lett.* **2002**, *81*, 1303.
[19] V. C. Sundar, H. J. Eisler, T. Deng, Y. T. Chan, E. L. Thomas, M. G. Bawendi, *Adv. Mater.* **2004**, *16*, 2137.
[20] P. T. Snee, Y. H. Chan, D. G. Nocera, M. G. Bawendi, *Adv. Mater.* **2005**, *17*, 1131.
[21] H. Takeuchi, H. Sakata, *Laser Phys. Lett.* **2008**, *5*, 41.
[22] J. Wang, T. Weimann, P. Hinze, G. Ade, D. Schneider, T. Rabe, T. Riedl, Y. Kowalsky, *Microelectron. Eng.* **2005**, *78–79*, 364.
[23] M. D. McGehee, M. A. Diaz-Garcia, F. Hide, R. Gupta, E. K. Miller, D. Moses, A. J. Heeger, *Appl. Phys. Lett.* **1998**, *72*, 1536.
[24] L. Shi, G. X. Zhang, J. Wang, D. Lo, *J. Opt. A: Pure Appl. Opt.* **2003**, *5*, L1.
[25] J. van Embden, P. Mulvaney, *Langmuir* **2005**, *21*, 10226.
[26] J. Jasieniak, L. Smith, J. van Embden, P. Mulvaney, M. Califano, *J. Phys. Chem. C* **2009**, *113*, 19468.
[27] G. A. Crosby, J. N. Demas, *J. Phys. Chem.* **1971**, *75*, 991.
[28] J. Jasieniak, J. Pacifico, R. Signorini, A. Chiasera, M. Ferrari, A. Martucci, P. Mulvaney, *Adv. Funct. Mater.* **2007**, *17*, 1654.
[29] J. J. Jasieniak, I. Fortunati, S. Gardin, R. Signorini, R. Bozio, A. Martucci, P. Mulvaney, *Adv. Mater.* **2008**, *20*, 69.
[30] J. C. de Mello, H. F. Wittmann, R. H. Friend, *Adv. Mater.* **1997**, *9*, 230.
[31] B. Xing, W. W. Li, K. Sun, *Mater. Lett.* **2008**, *62*, 3178.
[32] M. Rumi, J. E. Ehrlich, A. A. Heikal, J. W. Perry, S. Barlow, Z. Y. Hu, D. McCord-Maughon, T. C. Parker, H. Rockel, S. Thayumanavan, S. R. Marder, D. Beljonne, J. L. Bredas, *J. Am. Chem. Soc.* **2000**, *122*, 9500.
[33] M. Sheik-Bahae, A. A. Said, T.-H. Wei, D. J. Hagan, E. W. Van Stryland, *IEEE J. Quantum Electron.* **1990**, *26*, 760.
[34] G. S. He, Q. D. Zheng, K. T. Yong, A. I. Ryasnyanskiy, P. N. Prasad, A. Urbas, *Appl. Phys. Lett.* **2007**, *90*, 181108.
[35] C. Zhang, F. Zhang, T. Zhu, A. Cheng, J. Xu, Q. Zhang, S. E. Mohney, R. H. Henderson, Y. A. Wang, *Opt. Lett.* **2008**, *33*, 2437.
[36] R. Signorini, C. Ferrante, D. Pedron, M. Zerbetto, E. Cecchetto, M. Slaviero, I. Fortunati, E. Collini, R. Bozio, A. Abbotto, L. Beverina, G. A. Pagani, *J. Phys. Chem. A* **2008**, *112*, 4224.
[37] V. I. Klimov, A. A. Mikhailovsky, S. Xu, A. Malko, J. A. Hollingsworth, C. A. Leatherdale, H. J. Eisler, M. G. Bawendi, *Science* **2000**, *290*, 314.
[38] V. I. Klimov, *J. Phys. Chem. B* **2006**, *110*, 16827.
[39] V. I. Klimov, A. A. Mikhailovsky, D. W. McBranch, C. A. Leatherdale, M. G. Bawendi, *Science* **2000**, *287*, 1011.
[40] V. I. Klimov, *J. Phys. Chem. B* **2000**, *104*, 6112.
[41] H. Htoon, J. A. Hollingworth, A. V. Malko, R. Dickerson, V. I. Klimov, *Appl. Phys. Lett.* **2003**, *82*, 4776.
[42] M. Zavelani-Rossi, M. G. Lupo, R. Krahne, L. Manna, G. Lanzani, *Nanoscale* **2011**, *2*, 931.
[43] V. Klimov, S. Hunsche, H. Kurz, *Phys. Rev. B* **1994**, *50*, 8110.
[44] H. Kogelnik, C. W. Shank, *J. Appl. Phys.* **1972**, *43*, 2327.
[45] W. Holzer, A. Penzkofer, T. Pertsch, N. Danz, A. Brauer, E. B. Kley, H. Tillmann, C. Bader, H. H. Horhold, *Appl. Phys. B* **2002**, *74*, 333.
[46] G. Brusatin, G. Della Giustina, F. Romanato, M. Guglielmi, *Nanotechnology* **2008**, *19*, 175306.
[47] W. Holzer, A. Penzkofer, A. Lux, H. H. Horhold, E. B. Kley, *Synth. Met.* **2004**, *145*, 119.
[48] J. J. Li, Y. A. Wang, W. Z. Guo, J. C. Keay, T. D. Mishima, M. B. Johnson, X. G. Peng, *J. Am. Chem. Soc.* **2003**, *125*, 12567.
[49] J. van Embden, J. Jasieniak, D. E. Gomez, P. Mulvaney, M. Giersig, *Aust. J. Chem.* **2007**, *60*, 457.
[50] R. G. Xie, U. Kolb, J. X. Li, T. Basche, A. Mews, *J. Am. Chem. Soc.* **2005**, *127*, 7480.
[51] S. Dal Zilio, G. Della Giustina, G. Brusatin, M. Tormen, *Microelectron. Eng.* **2010**, *87*, 1143.
[52] C. Xu, R. M. Williams, W. Zipfel, W. W. Webb, *Bioimaging* **1996**, *4*, 198.
[53] E. Collini, C. Ferrante, R. Bozio, *J. Phys. Chem. C* **2007**, *111*, 18636.